Visible and NIR spectral analysis of Er^{3+} doped LiBiAlBSi glasses for laser applications

Mohit Kumar[1], Mukesh K. Sahu[1,3], Sumandeep Kaur[1], Aman Prasad[2], Rajat Bajaj[1], Rupesh A. Talewar[4], Yasha Tayal[1,5], K. Swapna[6], and A. S. Rao[1,*]

[1] Department of Applied Physics, Delhi Technological University, Bawana Road, New Delhi 110 042, India

[2] Department of Physics and Computer Science, Dayalbagh Educational Institute (DEI), Deemed University, Agra 282005, India

[3] Department of Electronics and Communication Engineering, GLA University, Mathura, Uttar Pradesh 281 406, India

[4] Department of Physics, Shri Ramdeobaba College of Engineering and Management, Katol Road, Nagpur 440013, India

[5] ABES Engineering College, Ghaziabad 201009, India

[6] Department of Engineering Physics, College of Engineering, Koneru Lakshmaiah Education Foundation, Vaddeswaram 522302, India

ABSTRACT

The lithium bismuth alumino borosilicate (LiBiAlBSi) glasses incorporated with different concentrations (0.1 to 2 mol%) of Er^{3+} ions were formed through the melt quench technique. Studies on optical absorption, photoluminescence, and decay profiles were performed. Detailed analysis of absorption and emission spectra was done by applying Judd- Ofelt (JO) theory. Under an excitation wavelength of 378 nm, the samples show intense green and NIR emission corresponding to transitions $^4S_{3/2} \rightarrow {}^4I_{15/2}$ (547 nm) and $^4I_{13/2} \rightarrow {}^4I_{15/2}$ (1538 nm), respectively. Dexter theory was applied to the NIR emission spectra to confirm the dipole–dipole nature of interaction among the Er^{3+} ions. CIE coordinates for the visible spectra lie in the green region. Various parameters such as stimulated emission cross-section, optical gain, and gain bandwidth for the as-prepared glasses show that these glasses exhibit good luminescence behavior and that the optimized LiBiAlBSiEr10 glass is ideal for laser applications in visible and NIR regions.

1 Introduction

Optically active luminescence glasses and phosphor materials attract the attention of scientists and researchers owing to their versatile applications in numerous fields such as telecommunication networks, solid-state laser, light-emitting diodes (LED), optical amplifiers, data storage devices, display monitors, and sensors [1–4]. In several of the aforesaid applications, the optical properties of the materials are improved by integrating Rare Earth (RE) (optically active) ions with different host materials. The RE ions show optical absorption and photoluminescence (PL) features due to the 4f transitions where 4f electrons are shielded from surrounding ligands and external interactions by the outermost electrons of the trivalent lanthanides. The RE elements have 5s and 5p electrons that surround 4f electrons and in this ways, 4f electrons get shielded from outer electrons. This leads to very less contributions of phonons i.e., weak lattice coupling

Ⓢ Springer

and negligible Stark splitting of the electronic states resulting in sharp luminescence. Among the RE ions, erbium (Er^{3+}) is suitable for several potential photonic applications such as gain media, visible lasers and near-infrared lasers, fiber amplifiers, temperature sensor, color displays etc. due to presence of the sharp spectral emissions in the Near Infra-Red (NIR) and visible region [5–7]. The glasses doped with Er^{3+} ions play a vibrant role in the expansion & development of telecommunication networks. Er^{3+} ions can be relevant specifically for eye-safe lasers due to the bands that exhibit in the NIR region. Extensive studies on RE ions doped glasses have been done in visible and NIR regions [4, 6, 8, 9].

Glasses as host materials can incorporate a large concentration of RE ions due to a good elastic matrix as compared to a crystalline host. The properties of glasses can be well optimized because their compositions, size, and shapes can be modified easily. Thus, glasses are a great choice as host materials to incorporate RE ions since their optical homogeneity is high, they have good thermal & mechanical stability along with the possibility of drawing the glasses into fiber form with low production cost. In this article, the borosilicate glass host is the combination of glass formers B_2O_3 and SiO_2 which have valuable qualities such as high mechanical strength, high thermal stability, and lower melting temperatures. Due to these beneficial properties, borosilicate glasses are utilized in innumerable fields of application [10–15]. But, relatively high phonon energy of borosilicate glasses leads to non-radiative losses resulting in loss of luminescence intensity [16, 17]. To reduce the non-radiative losses, the phonon energy is reduced by adding heavy metal bismuth oxide (Bi_2O_3) into the glass matrix which also plays an admirable role as a network former in addition to network modifier [18, 19]. Bi_2O_3 incorporated glasses have advantageous qualities such as higher infrared transparency, high density, higher refractive index (RI), and large dielectric constant. As spontaneous emission transition probability rises with RI, the high value of RI of bismuth deployed materials has considerable significance as a host material for luminous characteristics [20–22]. Al_2O_3 acts as glass network modifier and can improve luminescence properties of host matrix due to tetrahedral and octahedral Al^{3+} structural units. Al_2O_3 also helps in improving the chemical stability, thermo-mechanical stability along with the emission of the RE ions [13, 23, 24]. The addition of Li_2O modifies the glass network as it has a low thermal expansion, acceptable thermo-optical performance, and high thermal conductivity. So Li_2O decreases the thermal expansion coefficient and raises the transition temperature (T_g) of the glass matrix [1, 25]. In the light of above-mentioned properties, we have already studied lithium bismuth alumino borosilicate (LiBiAlBSi) glasses doped with Tb^{3+}, Sm^{3+} and codoped Sm^{3+}/Eu^{3+} ions [13, 16, 26]. The encouraging results from the above-mentioned studies motivated us to engage further in this glass host.

In the present work, we investigate LiBiAlBSi glass system doped with Er^{3+} ions to identify the optimized concentration of the Er^{3+} ions and determine the physical and optical properties using absorption spectrum, excitation spectrum, visible-NIR emission spectra and decay spectra analysis for their appropriateness in laser applications in visible and NIR regions.

2 Experimental

A series of different concentrations (0.1 to 2 mol%) of Er^{3+} ions incorporated LiBiAlBSi glasses was formed through melt quench technique. The composition of the glass is as follows:

$20Li_2CO_3$-$7.5Bi_2O_3$-$(7.5-x)$ Al_2O_3 $- 45H_3BO_3 -$ $20SiO_2 - x$ Er_2O_3 (x = 0.1 to 2.0 mol%).

As per concentration 0.1, 0.5, 1.0, 1.5, and 2.0 mol%, of Er^{3+} ions, the glasses have been labeled as LiBiAlBSiEr01, LiBiAlBSiEr05, LiBiAlBSiEr10, LiBiAlBSiEr15, and LiBiAlBSiEr20, respectively. The AR grade raw materials Li_2CO_3, Bi_2O_3, Al_2O_3, H_3BO_3, SiO_2 with high purity and Er_2O_3 of 99.99% purity were used for the synthesis of the glass samples. According to series composition, constituent chemicals were weighed for 7g batch, crushed, and mixed in an agate mortar using acetone as a wetting medium until a proper homogenous mixture was formed. This homogenous mix was then collected into silica crucible and kept in an electrical muffle furnace heated at 1150 °C for one hour until a uniform melt was obtained. A brass plate was kept at 350 °C for the purpose of quenching the melt. The melt was taken out of the furnace and poured on the preheated brass plate and quenched with another brass plate resulting in the formation of a transparent glass sample of uniform thickness and shape. The samples were circular in shape and had average thickness of approximately 0.13 cm. These obtained glasses were then annealed in an electrical furnace

for another 4 hours at 350 °C to relieve the glass from air bubbles and thermal strains.

The X-ray diffraction patterns were observed using X-ray diffractometer Bruker-Model D8. Archimedes' principle was used to measure the density of prepared glasses with water being used as immersion liquid in the measurement. All spectral measurements were done under ambient conditions. The UV-Vis-NIR spectrophotometer V-670 of JASCO was utilized to record absorption spectra. The excitation and NIR and visible photoluminescence (PL) spectra were taken in Photon Technology International QM-51 and Hitachi-F7000 fluorescence spectrophotometers. The PL decay profiles were measured with an Edinburgh FL920 fluorescence spectrometer which has an excitation source of Xenon flash lamp.

3 Result and discussion

3.1 X-ray diffraction pattern study

The diffraction patterns of undoped glass LiBiAlBSi and Er^{3+} doped glass LiBiAlBSiEr10 are illustrated in Fig. 1. X-ray diffraction patterns are not presenting any narrow and sharp peaks that suggests the absence of long-range order and supports an amorphous or non-crystalline nature of the prepared glasses [9, 27].
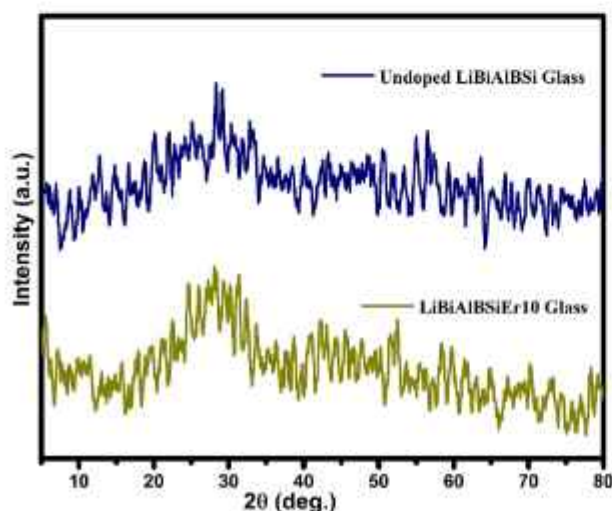
3.2 UV–Visible and NIR absorption spectrum

To attain the optical transitions characteristics, the absorption spectra of the LiBiAlBSi glasses incorporated with trivalent erbium ions was measured at ambient temperature in the range 350–1700 nm. Fig. 2 represents the absorption curve of the prepared glass sample LiBiAlBSiEr10 in UV–Visible and NIR region. Many absorption bands are seen because of the interactions between electrostatic and spin orbits of the f–f energy level of Er^{3+} ions. The absorption peaks were observed for the transitions from ground level $^4I_{15/2}$ to various upper levels $^4G_{11/2}$ (378 nm), $(^2G, ^4F)_{9/2}$ (408 nm), $^4F_{5/2}$ (453), $^4F_{7/2}$ (489 nm), $^2H_{11/2}$ (523 nm), $^4S_{3/2}$ (545 nm), $^4F_{9/2}$ (653 nm), $^4I_{9/2}$ (798 nm), $^4I_{11/2}$ (978 nm), and $^4I_{13/2}$ (1531 nm) of Er^{3+} ions .These peaks match well with data published by Carnall et al [28, 29]. The obtained spectrum peak positions are comparable to the reported literature signifying that Er^{3+} ions merge uniformly into the prepared glass network. The absorption intensity for the transition $^4I_{15/2} \rightarrow {}^4G_{11/2}$ (378 nm) is higher than other transitions in absorption spectra and follows $|\Delta J| \leq 2$, $|\Delta L| \leq 2$, and $|\Delta S| = 0$ selection rules. Therefore, this higher intensity transition is identified as hypersensitive transition since this transition is sensitive for host environment [30]. The inset of Fig. 2 presents the relationship of absorption intensity at 1531 nm peaks with Er^{3+} ions concentration. The absorption intensity increases almost linearly from 0.1 to 2.0 mol% concentration of Er^{3+} ions and
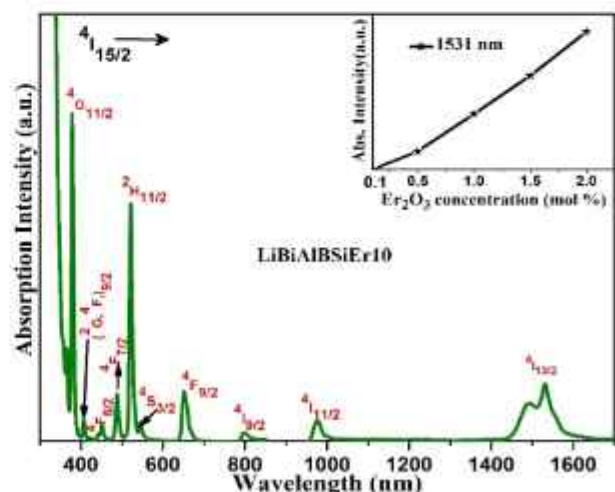

Fig. 1 XRD patterns of LiBiAlBSi and LiBiAlBSiEr10 glasses

Fig. 2 Absorption spectrum of the Er^{3+} ions doped LiBiAlBSiEr10 glass (inset: dependence of absorption intensity 1531 nm on the Er^{3+} ions concentration)

Springer

the shape of absorption peak at 1531 nm is not influenced by variation in Er^{3+} concentration. It means the crystal field in the host glass is controlled by the basic constituents of the host and not by the amount of Er^{3+} concentration [31].

The bonding nature among doped RE ions and oxygen ligands in the matrix of host glass is predicted by the nephelauxetic ratio $\left(\bar{\beta}\right)$ and bonding parameters (δ). The plus or minus sign before the bonding parameter (δ) predicts whether the bond is covalent or ionic in nature. The nephelauxetic ratio $\left(\bar{\beta}\right)$ and bonding parameter (δ) was estimated for all the attained transitions using the equations as mentioned below [28, 32, 33]:

$$\bar{\beta} = \frac{\nu_c}{\nu_a} \tag{1}$$

$$\delta = \frac{1 - \bar{\beta}}{\bar{\beta}} \tag{2}$$

In the above equations, ν_c and ν_a denote the wavenumbers of the transitions in complex and aqua-ion, respectively. The calculated values of Nephelauxetic ratio $(\bar{\beta})$ and bonding parameter (δ) for glass LiBiAlBSiEr10 are 0.999968 and + 0.00317, respectively. The positive value of δ means that the Er^{3+} ions share covalent bond with oxygen ligands in the host glass system.

3.2.1 Energy bandgap

The indirect optical energy bandgap (E_{opt}) was estimated by using the absorption spectra of Er^{3+} in LiBiAlBSi glasses. The fundamental absorption edge was used for the estimation of E_{opt} for LiBiAlBSi glasses incorporated with Er^{3+} ions by employing the equation of Davis and Mott [34, 35]:

$$\alpha h\nu = B\left(h\nu - E_{opt}\right)^m, \tag{3}$$

where α, ν, and B denote the absorption coefficient, frequency and the bond tailing parameter, respectively, whereas the index number m helps to determine the nature of the optical transition from absorption. The values of m can be 2 and 1/2 for indirect and direct permitted transitions, respectively. Generally, for oxide glasses, the indirect bandgap E_{opt} values were determined by the fitting of Tauc's plot in the linear region as represented in Fig. 3 and values of E_{opt} are given in

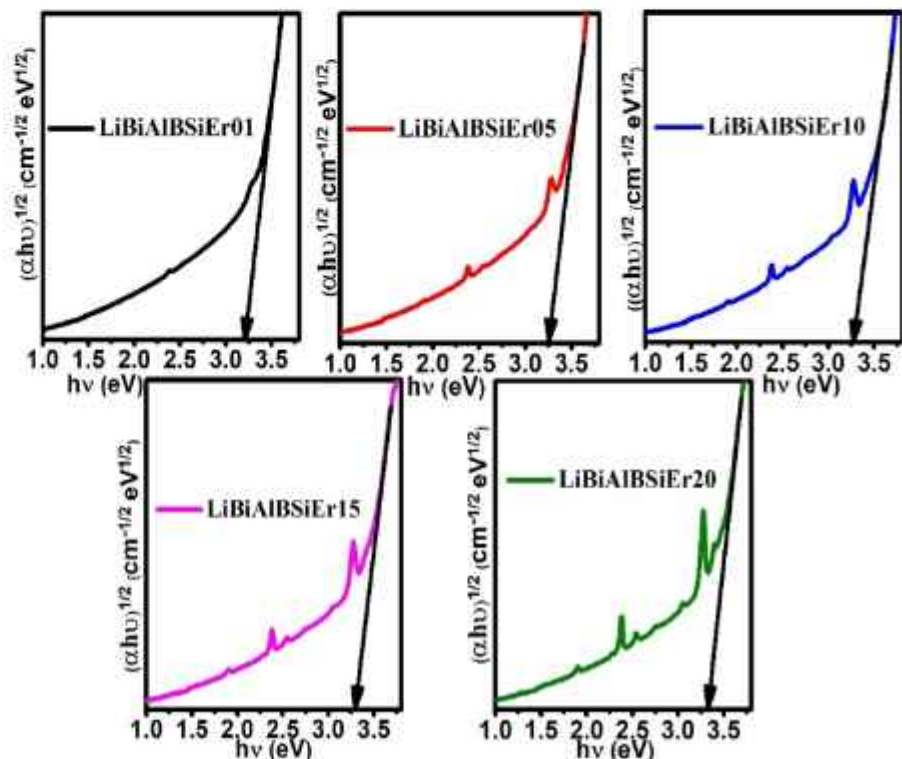Fig. 3 Indirect bandgap plot of Er^{3+} ions doped LiBiAlBSi glasses

Table 1. It can be seen that the indirect energy bandgap values are increasing (3.218 to 3.322 eV) with Er^{3+} concentration in the present glasses. This observed rise in the values of the energy bandgap may be because of the lessening of non-bridging oxygen (NBOs) in the glass matrix owing to oxygen binding variation. The reduction in NBOs lowers the valence band which leads to a surge in the values of E_{opt} [36]. Below the absorption edge region, α change as exponentially with the photon energy which denotes the presence of Urbach region. The Urbach region occurs due to the degeneracy of disorder in the amorphous material matrix and is measured in terms of Urbach energy (ΔE). The calculated values of ΔE tabulated in Table 1 by using the method used for other host glasses reported in published literature. The variation in the values of ΔE indicates the creation of defects in the matrix of as-prepared glasses [29, 37].

3.2.2 Refractive index and physical properties

The values of indirect E_{opt} were used for the estimation of the refractive index (n) for Er^{3+} doped LiBiAlBSi glasses by using the relation [38, 39]:

$$\frac{n^2 - 1}{n^2 + 2} = 1 - \sqrt{\frac{E_{opt}}{20}} \qquad (4)$$

The n values for LiBiAlBSi glasses doped with Er^{3+} ions are represented in Table 1 with the measured values of density and molar volume. The increasing values of density and decreasing values of molar volume & refractive index support the lessening of NBOs in as-prepared glasses by addition of Er^{3+} content [40, 41]. Some other physical parameters with the help of refractive index were identified for the LiBiAlBSiEr10 glass by using the certain equation explained elsewhere [32]. In Table 2 estimated physical parameters are tabulated with other reported Er^{3+} doped glasses BiBTEr1.0 [9], BLFBEr1 [42] and ZnAlBiBEr10 [4]. It is observed from Table 2 that the presented physical properties of LiBiAlBSiEr10 glass and the reported glasses in literature are comparable. Density is the property for the study of the modification of geometric configurations, degree of structural compactness and change in the coordination of glass networks. A refractive index is an effective tool for the investigation of optical materials. The solubility of RE ions is related to the field strength value and RE ions are highly soluble

Table 1 The optical band gap (E_{opt}), for indirect allowed transitions along with the refractive index of Er^{3+} ions in LiBiAlBSi glasses

Glass samples	Density gm/cm³	Molar Volume (V_m) (cm³/mol)	Indirect E_{opt} (eV)	Urbach energies ΔE(eV)	Refractive Index(n)
LiBiAlBSiEr01	3.478	28.030	3.218	0.2968	2.341
LiBiAlBSiEr05	3.531	27.927	3.237	0.2954	2.336
LiBiAlBSiEr10	3.634	27.521	3.261	0.2943	2.330
LiBiAlBSiEr15	3.692	27.292	3.292	0.2915	2.322
LiBiAlBSiEr20	3.751	27.411	3.322	0.2912	2.315

Table 2 Physical properties of the LiBiAlBSiEr10 glass along with other reported glasses

Physical properties	LiBiAlBSiEr10 [Present]	BiBTEr1.0 [9]	BLFBEr1 [42]	ZnAlBiBEr10 [4]
Density, d (g/cm³)	3.634	3.777	3.47	3.904
Refractive index, n	2.330	1.741	1.781	1.816
Average molecular weight(g)	100.01	137.8	76.261	114.4
Dielectric constant(ϵ)	5.428	3.031	3.172	3.297
Optical dielectric constant (ϵ-1)	4.428	2.031	–	2.279
Polaron radius, r_p (Å)	1.44	1.582	5.035	1.187
Inter-atomic distance,r_i (Å)	3.575	3.927	12.497	2.945
Molecular electronic polarizability α (10^{-23} cm³)	0.651	0.584	0.195	0.250
Field Strength, F (10^{15} cm⁻²)	14.456	11.976	2.37	21.28

Springer

in the present glass host matrix as the calculated value of field strength is low. Molecular electronic polarizability is correlated to various properties such as dielectric properties, ionic refraction, optical UV absorption and chemical stability. The chemical stability of material has an inverse relation with the value of molecular electronic polarizability [43–45]. The present glass system has low value of molecular electronic polarizability which shows its good stability.

3.2.3 Judd–Ofelt (JO) analysis

JO theory [46, 47] has been recognized to evaluate the JO intensity parameters $(\Omega_2, \Omega_4, \Omega_6)$ and various radiative properties of the glasses. The JO parameters evaluated using oscillator strength determined experimentally were discussed thoroughly in our earlier paper [16]. The values of oscillator strength were estimated by describing the absorption spectral intensities of the f-f transitions of the LiBiAlBSi glasses doped with the Er^{3+} ions. The experimental oscillator strength (f_{exp}) was calculated with the help of the area under the absorption peak for the corresponding absorption transition by following the equation described in the literature and the calculated oscillator strength (f_{cal}) was assessed by using the JO theory [30]. The values of f_{exp} and f_{cal} oscillator strengths of absorption transitions in LiBiAlBSiEr10 glass are presented in Table 3 along with the transitions, transition energies, band positions and root

mean square deviation (δ_{rms}) values. Relatively less value of the root mean square deviation (δ_{rms}) shown in Table 3 predict the better quality of fit between the experimental and calculated oscillator strengths and validity of JO analysis. It is noticed from Table 3 that $^4I_{15/2} \rightarrow \,^4G_{11/2}, \,^2H_{11/2}$ transitions show much higher values of oscillator strength when compared with other transitions. This is due to the enrichment of asymmetry nature which upsurges the possibility of emission in our prepared glasses and hence, the electrons oscillate at greater transition strengths [48]. In general, the values of JO intensity parameters are correlated with the local environment around trivalent rare-earth ions which affect the radiative transition properties. JO parameters were used to explain the symmetry, bonding nature, and rigidity of the present glass system.

The JO intensity parameters $(\Omega_{\lambda=2, 4, 6})$ of LiBiAlBSiEr10 glass are represented in Table 4. The Ω_2 parameter is associated with the bonding nature and sensitivity towards the local environment among the surrounding ligand and the RE ions positions [30]. Table 4 is also predicting the covalent characteristic between RE ions and ligand bond for the as-prepared glass as it shows the higher value of the Ω_2. Other JO parameters Ω_4 and Ω_6 are less sensitive to the local atmosphere and are related to the viscosity and rigidity of the host glass matrix [4]. From Table 4, the less values of Ω_4 and Ω_6 are advantageous for good luminescence characteristics and the revealed trend $\Omega_2 > \Omega_6 > \Omega_4$ may predict good quality luminescence of LiBiAlBSiEr10 glass system for the applications as optical devices [9, 49]. The JO parameters of the LiBiAlBSi Er10 glass and the other reported Er^{3+} ion-doped glasses PKAZFEr10 [2], LBTAFEr10 [7], BiBTEr1.0 [9], BLFBEr1 [42], and ZBLANP [50] are tabulated in Table 4. All show a similar trend $\Omega_2 > \Omega_6 > \Omega_4$.

Table 3 Transitions, transition energies (λ, nm), experimental (f_{exp}) and calculated (f_{cal}) oscillator strengths for LiBiAlBSiEr10 glass

Transition from $^4I_{15/2}$	λ (nm)	Oscillator strengths ($\times 10^{-6}$)	
		f_{exp}	f_{cal}
$^4G_{11/2}$	378	17.1872	18.7624
$(^2G,^4F)_{9/2}$	408	0.623	2.0405
$^4F_{5/2}$	453	0.854	1.8015
$^4F_{7/2}$	489	2.1577	4.795
$^2H_{11/2}$	523	12.0396	10.5738
$^4S_{3/2}$	545	2.47	1.4817
$^4F_{9/2}$	653	3.1	2.8849
$^4I_{9/2}$	798	0.421	0.1272
$^4I_{11/2}$	978	1.28	1.6838
$^4I_{13/2}$	1531	4.0333	3.5712
$\delta rms \times 10^{-6}$		± 1.264	

Table 4 Judd–Ofelt Parameters $(\Omega_\lambda \times 10^{-20} cm^2)$ of LiBiAlBSiEr10 glass along with reported values in literature

Glass System	Ω_2	Ω_4	Ω_6	Trend	References
LiBiAlBSiEr10	3.94	0.21	2.04	$\Omega_2 > \Omega_6 > \Omega_4$	present work
PKAZFEr10	8.23	1.04	1.91	$\Omega_2 > \Omega_6 > \Omega_4$	[2]
LBTAFEr10	5.89	1.10	1.47	$\Omega_2 > \Omega_6 > \Omega_4$	[7]
BiBTEr1.0	11.99	2.22	3.54	$\Omega_2 > \Omega_6 > \Omega_4$	[9]
BLFBEr1	3.53	0.64	1.68	$\Omega_2 > \Omega_6 > \Omega_4$	[42]
ZBLANP	3.08	1.50	1.71	$\Omega_2 > \Omega_6 > \Omega_4$	[50]

3.3 Photoluminescence (PL) analysis and radiative properties

3.3.1 Excitation spectrum

In order to study PL characteristics of erbium incorporated LiBiAlBSi glasses, the excitation spectrum of the LiBiAlBSiE10 glass sample has been observed in the wavelength range 200–1050 nm with emission wavelength 1538 nm and depicted in Fig. 4. The excitation spectrum reveals the following peak positions at wavelengths 368, 378, 407, 451, 489, 523, 546, 653, 804, and 980 nm corresponding to transitions from level $^4I_{15/2}$ (ground) to excited levels $^4G_{9/2}$, $^4G_{11/2}$, $(^2G, ^4F)_{9/2}$, $^4F_{5//2}$, $^4F_{7/2}$, $^2H_{11/2}$, $^4S_{3/2}$, $^4F_{9/2}$, $^4I_{9/2}$, and $^4I_{11/2}$, respectively [28]. The transition ($^4I_{15/2} \rightarrow ^4G_{11/2}$) at wavelength 378 nm is most intense and therefore, it has been used as an excitation wavelength (λ_{ex}) for recording emission spectra for all Er^{3+} ions doped LiBiAlBSi glasses.

3.3.2 Visible emission spectral study

The emission spectra were measured under excitation 378 nm at room temperature in the visible range from 500 to 650 nm and shown in Fig. 5(a) for the above-mentioned glasses. Three emission peaks of Er^{3+} ions are seen and assigned to the transitions: $^2H_{11/2} \rightarrow ^4I_{13/2}$ (527 nm), $^4S_{3/2} \rightarrow ^4I_{15/2}$ (547 nm) and $^4F_{9/2} \rightarrow ^4I_{15/2}$ (639 nm). Among all the three transitions, the green transition $^4S_{3/2} \rightarrow ^4I_{15/2}$ (547 nm) is found to be most intense. The emission peak intensity rises till 1 mol %
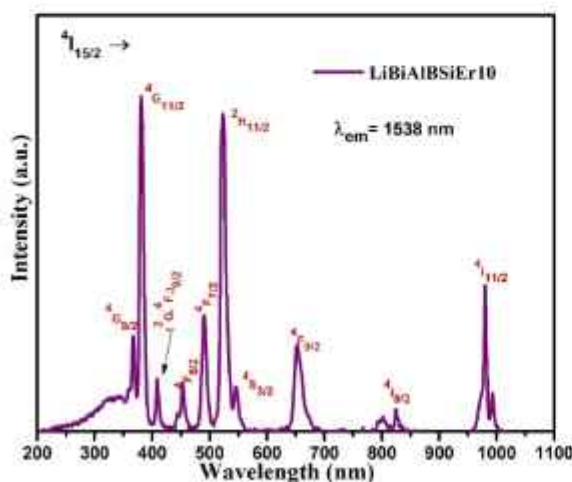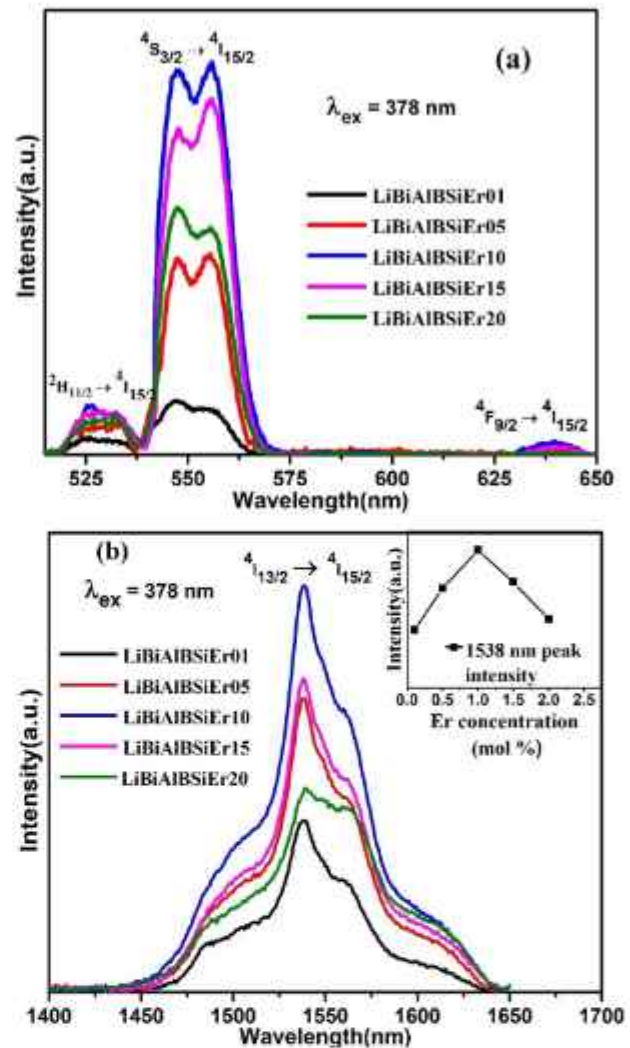
Fig. 5 Luminescence spectra of Er^{3+} ion-doped LiBiAlBSi glasses in (**a**) visible region (**b**) NIR region (inset: Variation of the emission intensity of transition $^4I_{13/2} \rightarrow ^4I_{15/2}$ at 1538 nm with $Er.^{3+}$ ions concentration)

and after that intensity shows decrement due to the quenching effect. The inter-ionic distance decreases between adjacent Er^{3+} ions with increment in their molar concentration which increases the possibility of non-radiative energy transfer through the mechanism of cross-relaxation, resulting in diminishing of emission intensity at higher concentration of Er^{3+} ions [9, 29]. Judd–Ofelt (JO) theory is a semi-empirical method that is used to evaluate the various spectroscopic radiative parameters as radiative branching ratio (β_R), transition probability (A) and radiative lifetimes (τ_R) of the upper levels of RE ions doped glasses with the spectral data of absorption & PL emission.

Fig. 4 The excitation spectrum of the Er^{3+} ions doped LiBiAlBSiEr10 glass

The β_R is a significant parameter for emission transition to describe the lasing power and its value should be greater than 0.5 for potential laser application [51]. The radiative parameters for LiBiAlBSiEr10 glass for the transition $^4S_{3/2} \rightarrow \, ^4I_{15/2}$ are estimated by using the expression in the literature [52]. The values of A, τ_R and β_R of $^4S_{3/2} \rightarrow \, ^4I_{15/2}$ transition are obtained as 7419.08 s^{-1}, 91 µs, and 0.676, respectively. The high intensity of green luminescence along with large value of transition probability and branching ratio allow us to conclude that our optimized LiBiAlBSiEr10 glass is an appropriate candidate for the applications of green laser action.

3.3.3 Near infra-red (NIR) emission spectral study

The emission spectra were recorded under excitation 378 nm in the NIR region from 1400 to 1650 and shown in Fig. 5(b). The graph has one broad emission peak at 1538 nm wavelength corresponding to transition $^4I_{13/2} \rightarrow \, ^4I_{15/2}$. The transition $^4I_{13/2} \rightarrow \, ^4I_{15/2}$ has received significant attention because of its feasibility in infrared laser, communication and range determination eye-safe laser applications [29]. The inset in Fig. 5(b) depicts the variation of emission intensity at 1538 nm with Er^{3+} concentration. LiBiAlBSiEr10 glass has highest intensity and after that, the luminescence intensity decreases due to concentration quenching just like the case with visible emission spectra. This is due to the non-radiative energy transfer mechanisms or multipole-multipole interaction [53].

To investigate the type of interaction mechanism, Dexter's theory was applied to emission spectral profile. According to Dexter theory, three interaction mechanisms can be investigated depending on the type of inter-ionic interaction and are identified by the expression [13, 54]

$$\log\left(\frac{I}{x}\right) = c - \frac{S}{3}\log(x), \tag{5}$$

where I the emission intensity of $^4I_{13/2} \rightarrow \, ^4I_{15/2}$ obtained from Fig. 5(b), x is activator (Er^{3+}) concentration in mol, c is a constant and s is the fitting parameter. The values of s are 6 for dipole-dipole (d–d), 8 for dipole–quadrupole (d–q) and 10 for quadrupole–quadrupole (q–q) interaction. For higher concentrations, equation (5) is more accurate. Fig. 6 depicts the graphs of log (I/x) versus log(x) and parameter 's' is attained from the slope of a linear fitted plot from experimental data.
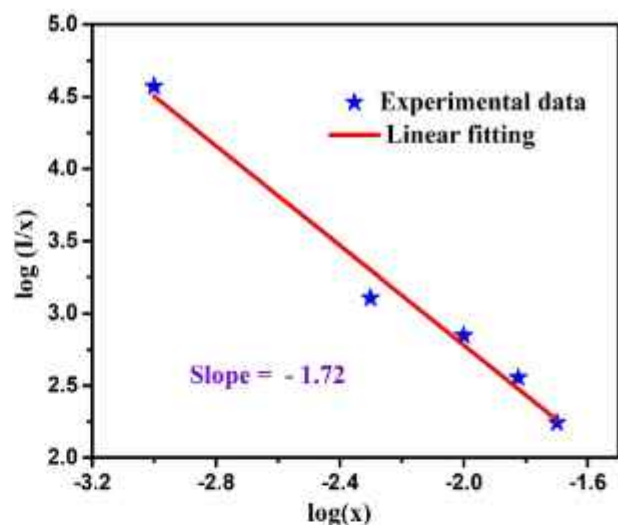
Fig. 6 Relation between log (I/x) and log (x) for different concentrations of Er^{3+}. Dexter model fitting shown by solid line

From Fig. 6 it can be seen that the slope is − 1.72 and the value of s is 5.16, which is nearly 6. This result indicated that the interaction among Er^{3+} ions is dipole-dipole in nature. The emission intensities decline above 1.0 mol% concentration of Er^{3+} ions due to the electric dipole-dipole interactions among the Er^{3+} ions.

From the NIR emission spectrum of optimized LiBiAlBSiEr10 glass for the $^4I_{13/2} \rightarrow \, ^4I_{15/2}$ transition the determined transition probability, branching ratio and radiative decay time were found to be 745 s^{-1}, 1.0 and 1342 µs, respectively. The value of transition probability is much higher than reported values. Another important factor to understanding for the efficacy of the RE ions doped materials for laser application from emission spectrum is stimulated emission cross-section (σ_{se}). This parameter determines the amount of energy withdrawn from the lasing material. σ_{se} value can be assessed by using the following expression [55]

$$\sigma_{se} = \frac{\lambda_p^4}{8\pi c n^2 \Delta\lambda p}A \tag{6}$$

where, λp, c, n and $\Delta\lambda_p$ are the emission peak wavelength, the light speed, the refractive index and transition effective bandwidth, respectively. In Table 5, radiative parameters such as peak wavelength (λp), branching ratio (β), effective bandwidths ($\Delta\lambda p$), transition probability (A), stimulated emission cross-sections (σ_{se}), optical gain parameter ($\sigma_{se} \times \tau_R$) and gain bandwidth ($\sigma_{se} \times \Delta\lambda p$) of LiBiAlBSiEr10 for the NIR transition $^4I_{13/2} \rightarrow \, ^4I_{15/2}$ (λp =1538 nm) are presented

Table 5 Emission peak wavelength λp (nm), effective bandwidths ($\Delta \lambda p$) (nm), branching ratio (β), transition probability (A) (s^{-1}), radiative lifetime (τ_R) (μs), stimulated emission cross-sections ($\sigma_{se} \times 10^{-20}$) (cm^2), gain bandwidth ($\sigma_{se} \times \Delta \lambda p \times 10^{-25}$) (cm^3) and optical gain parameter ($\sigma_{se} \times \tau_R \times 10^{-23}$) (cm^2 s) of 1.0 mol% Er^{3+} ions in LiBiAlBSi glass for the NIR emission transition $^4I_{13/2} \rightarrow {}^4I_{15/2}$ (λp =1538 nm) and compared with other reported glasses in literature for Er^{3+} doped glasses

Transition	Parameters	LiBiAlBSiEr10 [Present]	MBSER10 Ref [29]	BiBTEr1.0 Ref [9]	SAN-SCEr-10Ref [56]
$^4I_{13/2} \rightarrow {}^4I_{15/2}$	λp	1538	1536	1572	1535
	$\Delta \lambda p$	49.29	67	80	53
	β	1	1	1	1
	A	745.01	371.2	441.05	193
	τ_R	1342	2690	2260	5180
	σ_{se}	2.07	1.578	1.472	0.98
	$\sigma_{se} \times \Delta \lambda p$	1.02	1.057	1.178	0.52
	$\sigma_{se} \times \tau_R$	2.78	0.425	3.34	0.378

and compared with other glasses doped with Er^{3+} doped reported in the literature [9, 29, 56]. The optical gain ($\sigma_{se} \times \tau_R$) is an important parameter to evaluate the glass medium amplification for RE ions doped glasses. It is conspicuous from Table 5 that these radiative parameters have comparable values with other reported values which help concur that the optimized LiBiAlBSiEr10 glass is a possible applicant for optical amplifiers used in broadband.

Further, stimulated emission cross-section (σ_{em}) is estimated via employing the theory given by McCumbers [57]. As per the theory, the σ_{ab} can be evaluated by coupling absorption cross-section for $^4I_{13/2} \rightarrow {}^4I_{15/2}$ transition (1400–1700 nm range) in Er^{3+} ions given by the expression:

$$\sigma_{ab}(\vartheta) = \left[\frac{2.303 \times \log(\frac{I0}{I})}{N/l} \right] \quad (7)$$

In the above equation here, $\log(\frac{I0}{I})$ represents the optical density, N is the concentration of Er^{3+} ions in LiBiAlBSi glasses (ions/cm^3) and l denotes glass thickness. The $\sigma_{ab}(\vartheta)$ value expresses the efficiency of absorption for Er^{3+} ions. The stimulated emission cross-section (σ_{em}) can be obtained based on the $\sigma_{ab}(\vartheta)$ via using formula as [58]:

$$\sigma_{em}(\vartheta) = \sigma_{ab}(\vartheta) \left[\frac{\varepsilon - h\vartheta}{KT} \right] \quad (8)$$

In formula, ε signifies the energy to excite the Er^{3+} ions from $^4I_{15/2}$ level, K signifies Planck's constant and

ϑ demonstrations frequency of the photon. Figure 7 illustrates the σ_{em} and $\sigma_{ab}(\vartheta)$ profile by using McCumber's theory for optimized glass. Further, on the basis of σ_{em} and $\sigma_{ab}(\vartheta)$, the optical gain cross-section G (ϑ) was evaluated with varying population inversion parameter (γ) and signified as [59–61]

$$G(\vartheta) = \gamma \sigma_{em}(\vartheta) - (1 - \gamma)\sigma_{ab}(\vartheta) \quad (9)$$

Figure 8 represents G(ϑ) for different γ values of optimized glass. The prepared LiBiAlBSi glasses incorporated with Er^{3+} ions, the NIR emission spectra show a wide-ranging emission (1.45–1.65 μm) with a peak position at 1.538 μm thereby signifying the relevance of the present glass system in telecommunication
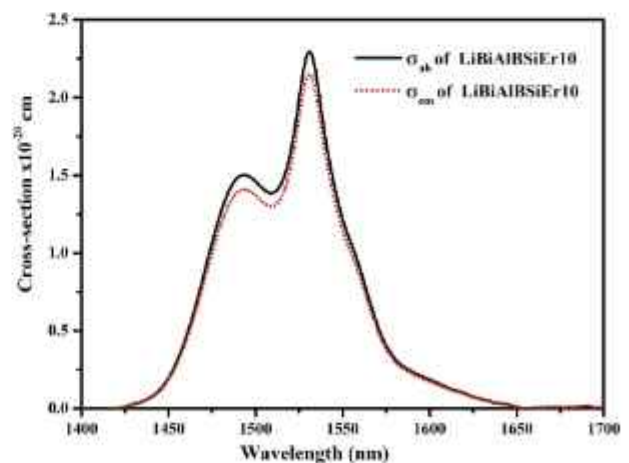
Fig. 7 Absorption and emission cross-sections of LiBiAlBSiER10 glass by McCumber theory
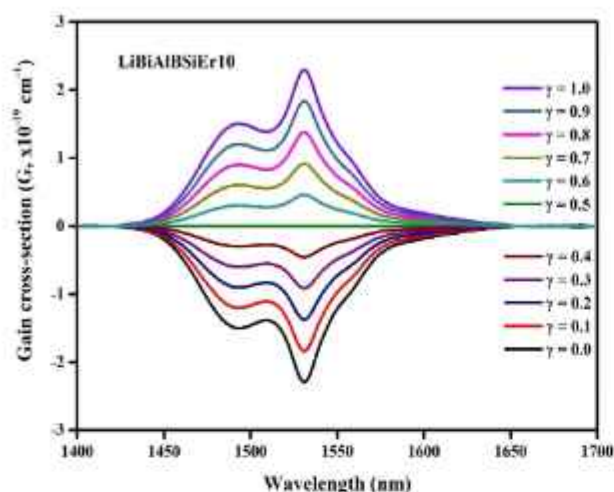
Fig. 8 The gain cross-section of LiBiAlBSiEr10 glass for different γ values

sector which covers optical communication bands such as Long (L), conventional (C) and, short (S) [29, 62].

To explain the mechanisms of excitation and emission, the partial energy level diagram of Er^{3+} doped glass LiBiAlBSiEr is shown in Fig. 9. When the glass was excited with 378 nm wavelength, the Er^{3+} ions move from the level $^4I_{15/2}$ (ground) to higher excited state $^4G_{11/2}$ These excited Er^{3+} ions, via non-radiative (NR) relaxations, fall to the levels $^2H_{11/2}$, $^4S_{3/2}$, $^4F_{9/2}$, and $^4I_{13/2}$ as shown in Fig. 9. After falling to these excited levels non-radiatively, the Er^{3+} ions fall to the ground state resulting in peaks in different regions of the spectra as shown in Fig. 9(a & b), respectively.

The strong NIR emission transition ($^4I_{13/2} \rightarrow {}^4I_{15/2}$) is detected at 1538 nm whereas visible transitions are observed at the peak wavelengths 639 nm, 527 nm, and 547 nm corresponding to the red, strong green and green emissions, respectively. These are the two possible regions where radiative emission of Er^{3+} ions can be observed under UV excitation as represented in energy level diagram.

3.4 Chromaticity color coordinates

For defining the colors, Commission Internationale de l'Eclairage (CIE) coordinates is a standard tool [27, 52]. The visible emission spectra of LiBiAlBSi glasses incorporated with Er^{3+} ions are used for evaluation of the CIE coordinates under excitation wavelength 378 nm and have been presented in Table 6. Fig. 10 shows the CIE coordinates value

Table 6 CIE chromaticity coordinates of Er^{3+} ions in LiBiAlBSi glasses under 378 nm excitation wavelength and Experimental lifetimes (τ_{exp}) (μs) for $^4S_{3/2} \rightarrow {}^4I_{15/2}$ (548 nm) transition of Er^{3+} ions in LiBiAlBSi glasses

Glass samples	x-coordinates	y-coordinates	τ_{exp}
LiBiAlBSiEr01	0.318	0.666	78.42
LiBiAlBSiEr05	0.316	0.677	76.67
LiBiAlBSiEr10	0.322	0.669	74.67
LiBiAlBSiEr15	0.332	0.659	69.17
LiBiAlBSiEr20	0.312	0.673	59.46

Fig. 9 Energy level diagram of 1.0 mol% Er^{3+} ions in LiBiAlBSi glass
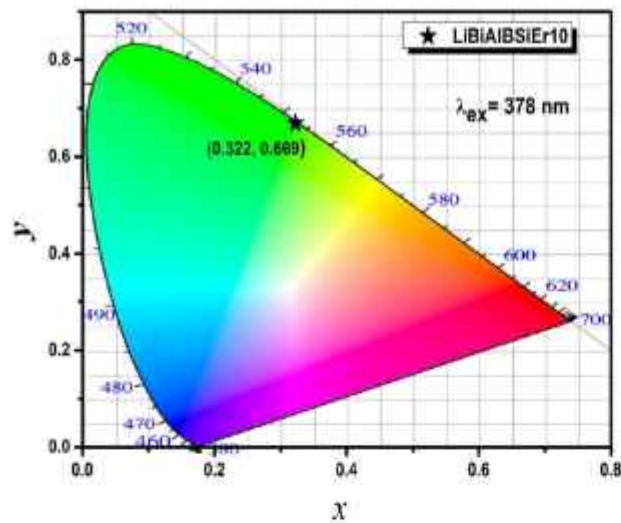
Fig. 10 CIE chromaticity coordinates of 1.0 mol% of Er^{3+} ions doped LiBiAlBSi glass

of optimum glass LiBiAlBSiEr10 (0.322, 0.669) in intense green region. Hence, glass LiBiAlBSiEr10 is an appropriate candidate for photonic applications in visible green regions.

3.5 Visible Fluorescence decay analysis

For all the as-prepared glasses, decay profiles were measured under excitation and emission wavelengths 378 nm and 547 nm, respectively. These decay profiles were recorded for characteristic green emission of Er^{3+} ions which initiates from excited level $^4S_{3/2}$ to lower level $^4I_{15/2}$. A bi-exponential function fitted well for the decay profiles which have been presented in Fig. 11. The emission intensity (I) of decay profiles can be shown by the expression [13, 63]

$$I = I_0 + a_1 \exp\left(-t/\tau_1\right) + a_2 \exp\left(-t/\tau_2\right), \qquad (10)$$

where intensities I_0 and I are at time $t = 0$ and $t = t$, respectively. The values a_1 and a_2 represent the decay constants amplitudes. τ_1 and τ_2 represent fast decay and slow decay times, respectively.

The average value of decay lifetime for the bi-exponential function is denoted by τ_{avg} and assessed by the equation

$$\tau_{avg} = \frac{a_1\tau_1^2 + a_2\tau_2^2}{a\tau_1 + a_2\tau_2} \qquad (11)$$

The τ_{avg} values of LiBiAlBSi glasses doped with Er^{3+} ions are represented in Table 6 as experimental

Fig. 11 Bi-exponential decay produced for $^4S_{3/2} \to {}^4I_{15/2}$ (547 nm) emission transition of Er^{3+} ions-doped LiBi-AlBSi glasses under 378 nm excitation
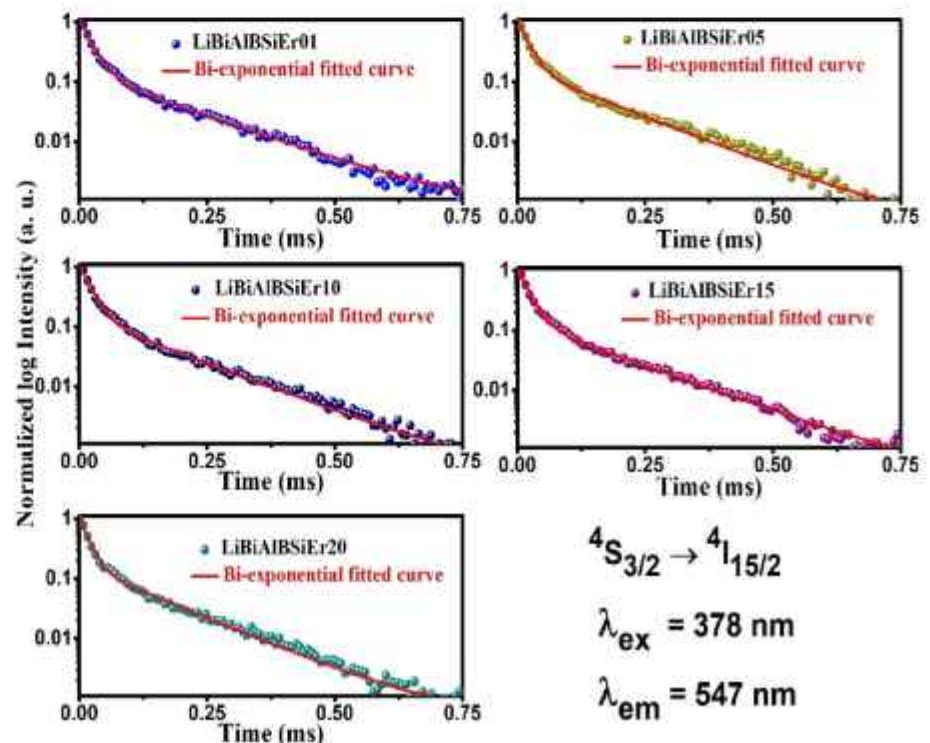
lifetime (τ_{exp}) in microseconds (µs). The values of τ_{exp} in Table 6 are decreasing from 78.72 to 59.46 µs with increasing Er^{3+} ions content from 0.1 to 2.0 mol%. The decline in lifetimes with an upsurge in the content of Er^{3+} ions is primarily due to the rise of energy transfer (ET) among Er^{3+} ions and ET from Er^{3+} ions to the impurities and other defects in the host.

4 Conclusions

The LiBiAlBSi glasses incorporated with different concentrations of Er^{3+} ions were synthesized via the melt quench method. These glasses have good transparency and optical quality. The indirect bandgap and JO parameters for the as-prepared glasses were calculated after analyzing the recorded absorption spectrum. The indirect energy bandgap values are increasing from 3.218 to 3.322 eV with increasing Er_2O_3 concentration. The bonding parameter (δ) and trend $\Omega_2 > \Omega_6 > \Omega_4$ of JO parameters indicate the predominance of covalent bonds between RE ions and ligand bond. Visible photoluminescence and strong NIR luminescence spectra were recorded under an excitation wavelength of 378 nm. The quenching effect is observed beyond 1.0 mol% of Er^{3+} ions signifying that LiBiAlBSiEr10 is the optimized glass and the radiative parameters were estimated for assessing the lasing features for this glass only. CIE color coordinates value for LiBiAlBSiEr10 is (0.332, 0.669) in the visible green region. Encouraging results from the study of radiative properties prove that the optimized glass system LiBiAlBSiEr10 is suitable for applications such as laser and optical amplifiers in the NIR region.

Author contributions

Mohit Kumar: Experimentation, data analysis, manuscript writing, Mukesh K. Sahu: Synthesis, experimentation, Sumandeep Kaur: data analysis, Aman Prasad: Manuscript Writing, review, data analysis, Rajat Bajaj: Experimentation, Rupesh A. Talewar: Data analysis, Yasha Tayal: Synthesis, experimentation, K. Swapna: Data analysis, review, A.S. Rao: Work Plan, review, supervision.

Data availability

The data that support the findings of this study are available on request from the corresponding author Prof. A.S. Rao. The data are not publicly available due to restrictions, e.g., their containing information that could compromise the privacy of research participants.

Declarations

Competing interests The authors declare that they have no known competing financial interests or personal relationships that could have appeared to influence the work reported in this paper.

References

1. J. Rajagukguk, B. Sinaga. Fitrilawati, J. Kaewkhao, Spectrochim. Acta A Mol. Biomol. Spectrosc **223**, 117342 (2019)

2. V.B. Sreedhar, N. Vijaya, D. Ramachari, C.K. Jayasankar, J. Mol. Struct. **1130**, 1001 (2017)

3. G.R. Dillip, C. Madhukar Reddy, M. Rajesh, S. Chaurasia, B.D.P. Raju, S.W. Joo, Bull. Mater. Sci. **39**, 711 (2016)

4. K. Swapna, S. Mahamuda, M. Venkateswarlu, A. Srinivasa Rao, M. Jayasimhadri, S. Shakya, G.V. Prakash, J. Lumin. **163**, 55 (2015)

5. A. Miguel, R. Morea, J. Gonzalo, M.A. Arriandiaga, J. Fernandez, R. Balda, J. Lumin. **140**, 38 (2013)

6. I.V. Kityk, V.V. Halyan, V.O. Yukhymchuk, V.V. Strelchuk, I.A. Ivashchenko, Y. Zhydachevskyy, A. Suchocki, I.D. Olekseyuk, A.H. Kevshyn, M. Piasecki, J. Non-Cryst, Solids. **498**, 380 (2018)

7. K.J.B.C. Jamalaiah, T. Suhasini, L. Rama Moorthy, K. Janardhan Reddy, Il-Gon. Kim, Dong-Sun. Yoo, Opt. Mater. **34**, 861 (2012)

8. B.V. Padlyak, R. Lisiecki, W. Ryba-Romanowski, Opt. Mater. **54**, 126 (2016)

9. Y. Anantha Lakshmi, K. Swapna, K.S.R.K. Reddy, M. Venkateswarlu, S. Mahamuda, A.S. Rao, J. Lumin. **211**, 39 (2019)

10. A.K. Varshneya, *Fundamentals of inorganic glasses* (Academic Press, Inc., Cambridge, 1993)

11. B.N.K. Reddy, B.D. Raju, K. Thyagarajan, R. Ramanaiah, Y.D. Jho, B.S. Reddy, Ceram. Int. **43**, 8886 (2017)

12. Y. Chu, J. Ren, J. Zhang, G. Peng, J. Yang, P. Wang, L. Yuan, Sci. Rep. **6**, 1 (2016)

13. M. Kumar, A.S. Rao, Opt. Mater. **120**, 111439 (2021)

14. A.S. Rao, J.L. Rao, V.V.R.K. Kumar, C.K. Jayasankar, S.V.J. Lakshman, Phys. Status Solidi B **174**, 183 (1992)

15. A.S. Rao, R. Ramakrishna, T.V. Ramakrishna, J.L. Rao, S. Krishnadevaraya, Solid State Commun. **96**, 701 (1995)

16. M. Kumar, A.S. Rao, Opt. Mater. **109**, 110356 (2020)

17. T. Yamashita, Y. Ohishi, J. Appl. Phys. (2007). https://doi.org/10.1063/1.2821789

18. E. Culea, L. Pop, S. Simon, Mater. Sci. Eng. B: Solid-State Mater. Adv. Technol. **112**, 59 (2004)

19. I. Ardelean, L. Griguta, J. Non-Cryst, Solids **353**, 2363 (2007)

20. M. Back, J. Ueda, M.G. Brik, T. Lesniewski, M. Grinberg, S. Tanabe, A.C.S. Appl, Mater. Interfaces **10**, 41512 (2018)

21. M. Back, E. Trave, N. Mazzucco, P. Riello, A. Benedetti, Nanoscale **9**, 6353 (2017)

22. T. Maeder, Int. Mater. Rev. **58**, 3 (2013)

23. J.E. Shelby, *Introduction to glass science and technology*, 2nd edn. (RSC, London, 2005)

24. Y.B. Saddeek, M.S. Gaafar, S.A. Bashier, J. Non-Cryst, Solids **356**, 1089 (2010)

25. S. Singh, G. Kalia, K. Singh, J. Mol. Struct. **1086**, 239 (2015)

26. M. Kumar, A.S. Rao, S. Kaur, Chem. Phys. Lett. **788**, 139303 (2022)

27. N. Deopa, M.K. Sahu, S. Kaur, A. Prasad, K. Swapna, V. Kumar, R. Punia, A.S. Rao, J. Rare Earths **39**, 520 (2021)

28. W.T. Carnall, P.R. Fields, K. Rajnak, J. Chem. Phys. **49**, 4424 (1968)

29. A. Jose, S. Gopi, T. Krishnapriya, T.A. Jose, C. Joseph, N.V. Unnikrishnan, P.R. Biju, Mater. Chem. Phys. **261**, 124223 (2021)

30. F. Ahmadi, R. Hussin, S.K. Ghoshal, J. Alloys Compd. **711**, 94 (2017)

31. S.F. Li, Q.Y. Zhang, Y.P. Lee, J. Appl. Phys. **96**, 4746 (2004)

32. A.S. Rao, Y.N. Ahammed, R.R. Reddy, T.V.R. Rao, Opt. Mater. **10**, 245–252 (1998)

33. S. P. Sinha, *Complexes of the Rare Earths*, 1st edn. (Pergamon Press, 1966).

34. N.F. Mott, E.A. Davis, Philos. Mag. **22**, 903 (1970)

35. R. Bajaj, A. Prasad, A.V.S. Yeswanth, P. Rohilla, S. Kaur, A.S. Rao, J. Mater. Sci.: Mater. Electron. **33**, 4782–4793 (2022)

36. C.R. Kesavulu, A.C. Almeida Silva, M.R. Dousti, N.O. Dantas, A.S.S. De Camargo, T. Catunda, J. Lumin. **165**, 77 (2015)

37. K. Annapoorani, K. Maheshvaran, S. Arunkumar, N. Suriya Murthy, K. Marimuthu, Spectrochim. Acta A Mol. Biomol. Spectrosc. **135**, 1090 (2015)

38. R. El-Mallawany, M.D. Abdalla, I.A. Ahmed, Mater. Chem. Phys. **109**, 291 (2008)

39. V. Dimitrov, S. Sakka, J. Appl. Phys. **79**, 1736 (1996)

40. H. Nurhafizah, M.S. Rohani, S.K. Ghoshal, J. Non-Cryst, Solids. **455**, 62 (2017)

41. P. Chimalawong, J. Kaewkhao, C. Kedkaew, P. Limsuwan, J. Phys. Chem. Solids **71**, 965 (2010)

42. K. Mariselvam, R. Arun Kumar, V. Rajeswara Rao, Opt. Laser Technol. **118**, 37 (2019)

43. S.A. Umar, M.K. Halimah, K.T. Chan, A.A. Latif, J. Non-Cryst, Solids. **472**, 31 (2017)

44. E.M. Ahmed, M.I. Youssif, A.A. Elzelaky, Ceram. Int. **45**, 24014 (2019)

45. S. Mahamuda, K. Swapna, P. Packiyaraj, A. Srinivasa Rao, G. Vijaya Prakash, J. Lumin. **153**, 382 (2014)

46. B.R. Judd, Phys. Rev. **127**, 750 (1962)

47. G.S. Ofelt, J. Chem. Phys. **37**, 511 (1962)

48. K. Maheshvaran, S. Arunkumar, V. Sudarsan, V. Natarajan, K. Marimuthu, J. Alloys Compd. **561**, 142 (2013)

49. Y.M. AbouDeif, E.S. Yousef, S.Y. Marzouk, J. Non-Cryst, Solids. **498**, 72 (2018)

50. T. Xue, C. Huang, L. Wang, Y. Li, Y. Liu, D. Wu, M. Liao, L. Hu, Opt. Mater. **77**, 117 (2018)

51. C. Madhukar Reddy, B.D.P. Raju, N. John Sushma, N.S. Dhoble, S.J. Dhoble, Renew. Sust. Energ. Rev. **51**, 566 (2015)

52. M.S. Sajna, S. Thomas, K.A. Ann Mary, C. Joseph, P.R. Biju, N.V. Unnikrishnan, J. Lumin. **159**, 55 (2015)

53. C. Nageswara Raju, C. Adinarayana Reddy, S. Sailaja, H.J. Seo, B. Sudhakar Reddy, Luminescence **27**, 334 (2012)

54. D.L. Dexter, J.H. Schulman, J. Chem. Phys. **22**, 1063 (1954)

55. N. Deopa, A.S. Rao, M. Gupta, G. Vijaya Prakash, Opt. Mater. **75**, 127 (2018)

56. G. Devarajulu, O. Ravi, C.M. Reddy, S.Z. Ali Ahamed, B.D.P. Raju, J. Lumin. **194**, 499 (2018)

Springer

57. D.E. McCumber, Phys. Rev. **134**, A299–A306 (1964)

58. L. Yuliantini, M. Djamal, R. Hidayat, K. Boonin, P. Yasaka, S. Kothan, J. Kaewkhao, J. Non-Cryst, Solids. **566**, 120849 (2021)

59. C.R. Kesavulu, H.J. Kim, S.W. Lee, J. Kaewkhao, N. Wantana, S. Kothan, S. Kaewjaeng, J. Alloys Compd. **683**, 590 (2016)

60. N. Luewarasirikul, S. Sarachai, M. Djamal, J. Kaewkhao, Optik **266**, 169557 (2022)

61. R. Rajaramakrishna, Y. Ruangtaweep, N. Sangwaranatee, J. Kaewkhao, J. Non-Cryst, Solids. **521**, 119522 (2019)

62. A.D. Sontakke, K. Biswas, A. Tarafder, R. Sen, K. Annapurna, Opt. Mater. Express **1**, 344 (2011)

63. M.K. Sahu, M. Jayasimhadri, J. Lumin. **227**, 117570 (2020)